Acta Crystallographica Section D
Biological Crystallography
ISSN 0907-4449

Suggestive evidence for the involvement of the second calcium and surface loop in interfacial binding: monoclinic and trigonal crystal structures of a quadruple mutant of phospholipase A_2

K. Sekar,[a,b]* M. Yogavel,[c] Shankar Prasad Kanaujia,[a,b]‡ Alok Sharma,[d] D. Velmurugan,[c] M.-J. Poi,[e] Z. Dauter[f] and M.-D. Tsai[e,g]

[a]Bioinformatics Centre, Indian Institute of Science, Bangalore 560 012, India, [b]Supercomputer Education and Research Centre, Indian Institute of Science, Bangalore 560 012, India, [c]Department of Crystallography and Biophysics, University of Madras, Guindy Campus, Chennai 600 025, India, [d]Molecular Biophysics Unit, Indian Institute of Science, Bangalore 560 012, India, [e]Departments of Chemistry and Biochemistry and the Ohio State Biochemistry Program, The Ohio State University, Columbus, OH 43210, USA, [f]Synchrotron Radiation Research Section, MCL, NCI, Argonne National Laboratory, Argonne, IL 60439, USA, and [g]Genomics Research Center, Academia Sinica, Taiwan

‡ Carried out docking studies.

Correspondence e-mail: sekar@physics.iisc.ernet.in, sekar@serc.iisc.ernet.in

Received 25 January 2006
Accepted 24 April 2006

PDB References:
K53,56,120,121M PLA_2, monoclinic, 2bd1, r2bd1sf; K53,56,120,121M PLA_2, trigonal, 2bch, r2bchsf.

The crystal structures of the monoclinic and trigonal forms of the quadruple mutant K53,56,120,121M of recombinant bovine pancreatic phospholipase A_2 (PLA_2) have been solved and refined at 1.9 and 1.1 Å resolution, respectively. Interestingly, the monoclinic form reveals the presence of the second calcium ion. Furthermore, the surface-loop residues are ordered and the conformation of residues 62–66 is similar to that observed in other structures containing the second calcium ion. On the other hand, in the trigonal form the surface loop is disordered and the second calcium is absent. Docking studies suggest that the second calcium and residues Lys62 and Asp66 from the surface loop could be involved in the interaction with the polar head group of the membrane phospholipid. It is hypothesized that the two structures of the quadruple mutant, monoclinic and trigonal, represent the conformations of PLA_2 at the lipid interface and in solution, respectively. A docked structure with a phospholipid molecule and with a transition-state analogue bound, one at the active site coordinating to the catalytic calcium and the other at the second calcium site, but both at the i-face, is presented.

1. Introduction

The enzyme phospholipase A_2 (PLA_2) is implicated in a variety of physiologically important cellular processes. It is found in many tissues, where it catalyzes hydrolysis of the fatty-acid ester bond at the *sn*-2 position of membrane phospholipids in a calcium-dependent reaction and therefore initiates inflammatory and platelet activities (Dennis, 1994). PLA_2 is involved in two major events: (i) interfacial binding or enzyme–membrane interaction and (ii) lipid hydrolysis at the active site. The active site is one of the important structural elements for the catalytic reaction of PLA_2 (Dijkstra *et al.*, 1984; Jain *et al.*, 1986; Scott *et al.*, 1990). Based on the three-dimensional crystal structures and on the results of chemical modification reactions, a detailed mechanism for the catalytic action has been proposed (Scott *et al.*, 1990). The interfacial binding site has been shown to involve the 'i-face' (Berg *et al.*, 2001); however, detailed structural features of the PLA_2–membrane binding remain unknown.

Biochemical studies of bovine pancreatic PLA_2 (Rogers *et al.*, 1998; Yu *et al.*, 2000) suggested that the lysine-to-methionine substitution of the residues 53, 56, 120 and 121 eliminates the anionic interface preference of the wild type. These four residues are located in two well separated regions of the molecule. Consequently, several structures of mutants involving these residues have been solved in our laboratory in the last few years. In the crystal structures of the double mutants

K53,56M (Yu *et al.*, 2000) and K120,121M (Huang *et al.*, 1996), no second calcium ion was noticed. However, interestingly, the crystal structure of the triple mutant K56,120,121M (Rajakannan *et al.*, 2002) revealed the unequivocal presence of the second calcium ion for the first time in bovine pancreatic PLA_2 enzyme. Subsequently, the atomic resolution structure of another triple mutant (K53,56,121M) was also shown to contain the second calcium ion (Sekar *et al.*, 2005). The crystal structures of these triple mutants containing the second calcium ion also showed distinct conformational variation in the surface loop involving residues 62–66 (Rajakannan *et al.*, 2002; Sekar *et al.*, 2005), as well as ordering of the surface loop (Fig. 1). In the structures of the wild type and of the mutants that do not contain the second calcium ion, the residues in the surface loop are disordered (Sekar *et al.*, 2003). The reason for the different behaviour of some of the mutants is not fully understood. However, as has been pointed out previously for porcine pancreatic PLA_2 (Thunnissen *et al.*, 1993), the surface loop is less well defined in water and in the absence of lipids and more ordered in the presence of a competitive inhibitor (Peters *et al.*, 1992). To probe the role of the second calcium ion and the surface-loop residues in interfacial binding, the crystal structure of the quadruple mutant K53,56,120,121M has been undertaken. The results of the quadruple mutant structures of both the monoclinic (1.9 Å resolution) and trigonal (1.1 Å resolution) forms are discussed in detail. A model of PLA_2 bound with two phospholipid molecules coordinated to both Ca atoms is proposed.

2. Materials and methods

2.1. Site-directed mutagenesis and protein purification

The quadruple mutant K53,56,120,121M was generated by using triple-mutant pET25b (m)-proPLA_2 (K53,120,121M) as template. The triple mutant in turn was made by using the corresponding double-mutant pET25b (m)-proPLA_2 as template. The oligonucleotides in complementary sets used are as follows: 5′-AACACAAGAATCTTGATATGATGAACTGTTAAGCTTCTG-3′ (K120,121 to M), 5′-TGCTATAAACAAGCTATGAAACTTGATAGCTGC-3′ (K56 to M) and 5′-CATGATAATTGCTATATGCAAGCTAAAAAACTT-3′ (K53 to M). The recombinant PLA_2 mutant was expressed in *Escherichia coli* BL21 (DE3) pLys S (Novagen) strain as inclusion-body protein, which was refolded as described previously (Deng *et al.*, 1990).

2.2. Crystallization

Lyophilized protein samples of the present quadruple mutant were dissolved in 50 m*M* Tris buffer pH 7.2 containing 5 m*M* $CaCl_2$ to a final protein concentration of 18–20 mg ml^{-1}. Crystals were obtained at room temperature (293 K) using the hanging-drop vapour-diffusion method and grew over a period of 10 d. For the monoclinic form, the crystallization droplet contained 5 µl protein solution and 2 µl 2-methyl-2,4-pentanediol [MPD; 60%(*v*/*v*)] pH 7.2 and the reservoir contained 70%(*v*/*v*) MPD. The trigonal form of the quadruple mutant was obtained from a droplet containing 5 µl protein solution and 2 µl 50% MPD; the reservoir contained 75% MPD.

2.3. Data collection, structure solution, model building and refinement details of the monoclinic form of the quadruple mutant

The intensity data of the monoclinic form were collected at room temperature (293 K) using a 300 mm MAR Research imaging-plate detector mounted on a Rigaku rotating-anode generator operated at 40 kV and 56 mA equipped with a Cu $K\alpha$ target. The crystal-to-detector distance was 100 mm. The diffraction data were processed to 1.9 Å resolution using the programs *DENZO* (Otwinowski, 1993) and *SCALEPACK* (Minor, 1993). The crystal was monoclinic (space group *C*2), with unit-cell parameters $a = 74.58$, $b = 48.69$, $c = 67.55$ Å, $\beta = 102.3^\circ$ (Table 1), and preliminary calculations revealed the presence of two molecules in the asymmetric unit. The structure was solved by the molecular-replacement method using the program *AMoRe* (Navaza, 1994). The high-resolution orthorhombic form (1.5 Å) of the recombinant PLA_2 (Sekar & Sundaralingam, 1999) was used as the starting model. Molecular-replacement calculations gave two independent solutions with high correlation coefficient (68%) and low *R*

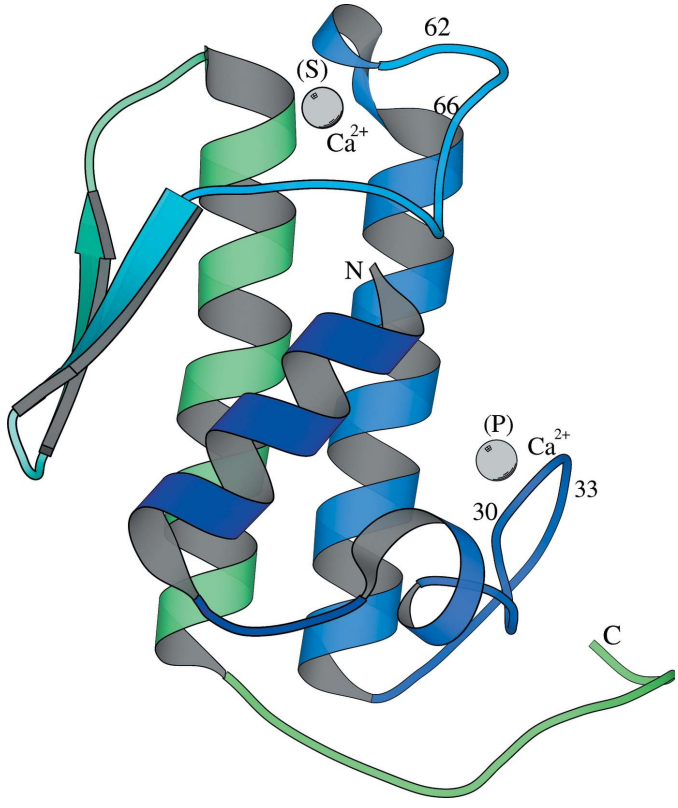

Figure 1
The tertiary structure of the monoclinic form of the quadruple mutant of recombinant PLA_2 showing the primary (P) and the secondary (S) calcium ions. The figure was produced using the program *MOLSCRIPT* (Kraulis, 1991). For clarity, only molecule *A* is shown here.

factor (38.5%). Refinement of the structure in the resolution range 14.7–1.9 Å without any σ cutoff was carried using the target function 'maximum-likelihood function' (m.l.f.), slow-cooling protocols and torsion-angle dynamics using *CNS* (Brünger *et al.*, 1998). The progress of the refinement was monitored and the quality of the model was checked throughout the refinement using a total of 1071 (7%) reflections (for the $R_{\rm free}$ value; Brünger, 1992). Initial refinement was carried out by completely omitting the four mutated residues (Met53, Met56, Met120 and Met121). 25 cycles of rigid-body refinement were initially carried out followed by 100 cycles of positional refinement and the $R_{\rm work}$ fell to 36.1% ($R_{\rm free}$ = 38.2%) for reflections in the resolution range 14.7–1.9 Å. Inspection of the first-round difference electron-density maps clearly revealed the density for the mutated methionine residues and these were fitted using the molecular-modelling program *FRODO* (Jones, 1985). In addition, five surface-loop residues (62–66) were refitted. These models were then subjected to simulated annealing by employing a slow-cooling protocol. $R_{\rm work}$ fell to 28.1% ($R_{\rm free}$ = 33.2%). The difference maps showed the electron density for the primary calcium ion in the active site. Interestingly, one large peak (peak height = 8σ) was found near the N-terminal region, exactly in the same place as found in the triple-mutant structures (Rajakannan *et al.*, 2002; Sekar *et al.*, 2005, 2006). This large peak was assigned as calcium ion (hereafter referred to as the second calcium ion). Water O atoms and two molecules of 2-methyl-2,4-pentanediol (MPD) were added using the difference electron-density maps. Water molecules were located using the difference map $|F_{\rm o}| - |F_{\rm c}|$ and included in the refinement wherever they satisfied the hydrogen-bonding distance (2.5–3.6 Å). The $2|F_{\rm o}| - |F_{\rm c}|$ map was also used to check the quality of the water peaks. In the course of further refinement, additional water molecules were picked and included in the refinement. The composite simulated-annealing omit maps, as implemented in the refinement program *CNS*, were calculated to check the final protein model. The final $R_{\rm work}$ was 20.7% ($R_{\rm free}$ = 24.0%) and the model consists of 246 residues (two molecules in the asymmetric unit), four calcium ions, two MPD molecules and 218 water O atoms. A total of 89% of the residues are in the most favoured regions of the Ramachandran plot (Laskowski *et al.*, 1993; Ramachandran & Sasisekharan, 1968). The remaining residues are in the additional (10%) and generously allowed regions (1%).

Table 1
Crystal and other relevant geometrical parameters of the monoclinic form of bovine pancreatic phospholipase A_2.

Values in parentheses are for the highest resolution shell.

PDB code	2bd1
Wavelength (Å)	1.54
Temperature (K)	293
Unit-cell parameters (Å, °)	a = 74.58, b = 48.69, c = 67.55, $\alpha = \gamma$ = 90, β = 102.3
$V_{\rm M}$ (Å^3 Da^{-1})	2.17
Z	4
Space group	$C2$
Resolution range (Å)	14.7–1.90 (1.97–1.90)
Unique reflections	13440 (1753)
Completeness of data (%)	94.7 (94.5)
$R_{\rm merge}$†	0.093 (0.453)
Protein atoms	1906
Calcium ions	4
MPD atoms	16
Water molecules	218
$R_{\rm work}$ (%)	20.7
$R_{\rm free}$ (%)	24.0
Ramachandran plot, residues in	
Most favoured regions (%)	89
Additionally allowed regions (%)	10
Generously allowed regions (%)	1
R.m.s. deviations	
Bond lengths (Å)	0.034
Bond angles (°)	4.1
Mean B factor (Å^2)	
All protein atoms	18.5
Main-chain atoms	18.0
Side-chain atoms	23.0
Water molecules	35.5
MPD molecules	41.2

† $R_{\rm merge} = \sum_{hkl} |I - \langle I\rangle| / \sum I$, where I is the observed intensity and $\langle I\rangle$ is the average intensity from observations of symmetry-related reflections.

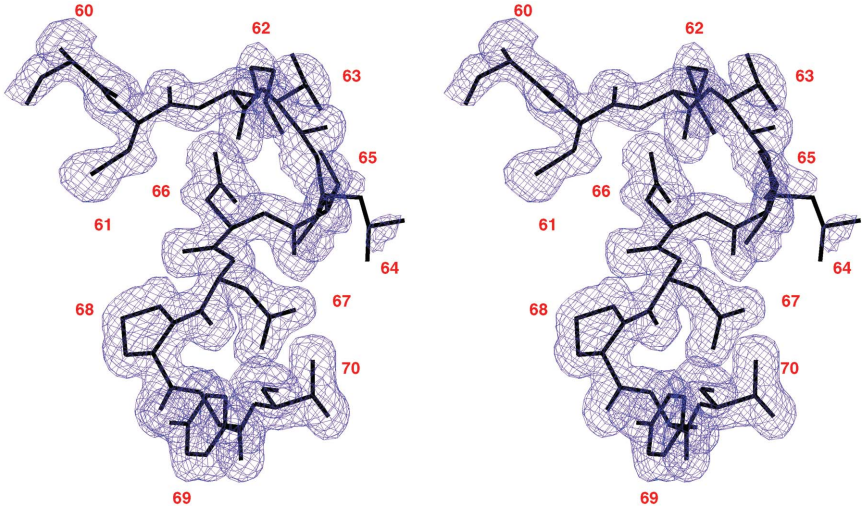

Figure 2
A stereoview of the omit electron-density map (molecule A) showing the ordered surface-loop residues 60–70 in the monoclinic form of the quadruple mutant contoured at the 1.0σ level.

2.4. Data collection, structure solution, model building and refinement details of the trigonal form of the quadruple mutant

The X-ray diffraction data of the trigonal form of the quadruple mutant were collected at cryotemperature (100 K) on beamline X9B at the National Synchrotron Light Source (Brookhaven National Laboratory, Upton, NY, USA) using an ADSC Quantum 4 CCD detector. The data were processed and scaled using the *HKL*2000 suite (Otwinowski & Minor, 1997). A summary of intensity data statistics

Table 2
Crystal and other relevant geometrical parameters of the trigonal from of bovine pancreatic phospholipase A_2.

Values in parentheses are for the highest resolution shell.

PDB code	2bch
Wavelength (Å)	0.979
Temperature (K)	100
Unit-cell parameters (Å, °)	$a = b = 45.908$, $c = 101.372$, $\alpha = \beta = 90$, $\gamma = 120$
V_M (Å^3 Da^{-1})	2.24
Z	6
Space group	$P3_121$
Resolution range (Å)	20.0–1.10 (1.14–1.10)
Unique reflections	50486 (4723)
Completeness of data (%)	98.8 (94.2)
R_{merge}	0.045 (0.473)
Protein atoms	953 (267 partial occupancies)
Calcium ions	1
Chloride ions	1
MPD atoms	96
Water molecules	253
R_{work} for $F > 4\sigma$ (%)	10.55
R_{free} for $F > 4\sigma$ (%)	13.50
R_{work} for all data (%)	11.96
Ramachandran plot, residues in	
Most favoured regions (%)	89.1
Additionally allowed regions (%)	10.9
R.m.s. deviations	
Bond distances (Å)	0.013
Bond-angle distances (Å)	0.034
Mean B factor (Å^2)	
All protein atoms	21.34
Main-chain atoms	19.21
Side-chain atoms	23.29
Water molecules	31.69
MPD molecules	28.27

is given in Table 2. The structure was solved with the molecular-replacement program *EPMR* (Kissinger *et al.*, 1999) using the atomic coordinates of the orthorhombic form (PDB code 1une; Sekar & Sundaralingam, 1999) and could be refined directly. For the refinement process, the programs *SHELXL*97 (Sheldrick & Schneider, 1997) and *SHELXPRO* were used. A randomly selected 2519 (5%) of the data were set aside for R_{free} calculations (Brünger, 1992). The *SHELXL*97 default restraints and their weights were used for protein geometry (Engh & Huber, 1991) and SIMU was set as 0.05 instead of the default 0.1 for anisotropic displacement parameters. The model was initially refined using full-matrix least-squares rigid-body refinement and was subsequently subjected to isotropic refinement using the conjugate-gradient least-squares (CGLS) mode (resolution range extended to 20.0–1.1 Å). Two rounds of 20 cycles of CGLS refinements were carried out. The water and MPD molecules were located during the progress of the refinement. The isotropic refinement led to R_{work} and R_{free} values of 22.9 and 25.4%, respectively. Introduction of anisotropic displacement parameters reduced R_{work} (15.1%) and R_{free} (18.5%) significantly. The quality of the electron-density map permitted the modelling of alternate conformations of several main-chain and side-chain atoms. The occupancy of the double conformation was refined individually, with the sum of the occupancies of corresponding atoms being set to unity. Partially occupied water sites were adjusted manually depending on the refined B factors. After minor adjustments of the model, the anisotropic refinement converged to 11.4% (R_{work}) and 15.1% (R_{free}). H atoms were included at their idealized positions and those of the hydroxyl groups were also generated automatically, but their locations were verified manually for consistency and plausible hydrogen-bonding interactions. In the final round of refinement, all the test reflections used for the calculation of R_{free} were included and the crystallographic R value converged to 10.6% [for 39 945 reflections with $F_o > 4\sigma(F_o)$].

3. Results and discussion

3.1. Details of the monoclinic structure

In the final refined protein model, there are 1906 non-H atoms (246 amino-acid residues), 218 water O atoms, four calcium ions and two MPD (2-methyl-2,4-pentanediol) molecules. The relevant data-collection and refinement statistics are given in Table 1. Fig. 1 shows the secondary-structural elements of bovine pancreatic PLA_2, the catalytically important primary calcium ion (P) and the second calcium ion (S). The backbone atoms (492) of molecule A superimpose very well with the corresponding atoms of molecule B with a root-mean-square deviation (r.m.s.d.) of 0.08 Å. The molecule B is translated by 11.8 Å along the unique axis with a rotation of 0.02° with respect to molecule A. Hence, we confine ourselves to molecule A for comparison with the other forms of PLA_2 structures in the rest of the paper. The superposition of the backbone atoms of the present structure with the monoclinic form of the triple mutant (Rajakannan *et al.*, 2002) and with the orthorhombic form (Sekar & Sundaralingam, 1999) gives an r.m.s.d. of 0.50 and 1.05 Å, respectively. The corresponding value with the trigonal form (Sekar, Sekharudu *et al.*, 1998) is 1.2 Å and the largest deviations are observed in the surface-loop residues (60–70) and in the C-terminal region (residues 116–123). If these residues are omitted from the superposition, the r.m.s.d. reduces to 0.58 and 0.57 Å with the trigonal and orthorhombic forms, respectively. The electron density is very clear for all the residues (60–70) in the surface loop (Fig. 2). The catalytically important primary calcium ion has seven ligands that exhibit pentagonal bipyramidal coordination and the ligand distances vary between 2.31 and 2.58 Å, with an average of 2.42 Å. As noted in the triple mutants K56,120,121M (Rajakannan *et al.*, 2002) and K53,56,121M (Sekar *et al.*, 2005), an additional calcium ion (second calcium) was identified (Fig. 3) in both molecules A and B (see discussion below). The ligands of the second calcium ion include one of the carboxylate O atoms ($O^{\epsilon 2}$) of Glu 92, $O^{\delta 1}$ of Asn71, the backbone O atom of Asn72 and three water molecules. The electron density is very clear for all coordinating ligands and the average calcium–ligand distance is 2.44 Å for molecule A and 2.43 Å for molecule B. The average distance agrees well with the distances observed with the other structures (Rajakannan *et al.*, 2002; Sekar *et al.*, 2005).

Of the 218 water molecules (186 are in the primary hydration shell) located in the medium-resolution model, 116 and 99

water O atoms belong to molecules *A* and *B*, respectively. These water molecules make 282 and 262 contacts with molecules *A* and *B*, respectively (Shanthi *et al.*, 2003). The primary hydration-shell water molecules make 190 and 154 hydrogen bonds (<3.6 Å) with the polar atoms of the main chain and side chain, respectively (Thanki *et al.*, 1988) A total of 20 water molecules lie in the interface of molecules *A* and *B*; of these, nine water molecules are hydrogen bonded to molecule *A* and the rest are bonded to molecule *B*. 70 water molecules are invariant/common between molecules *A* and *B*.

3.2. Details of the trigonal structure

The Ramachandran plot (Ramachandran & Sasisekharan, 1968) calculated by the program *PROCHECK* (Laskowski *et al.*, 1993) shows 89.1% of the residues in the most favoured regions and the remainder in additionally and generously allowed regions. The primary calcium-binding loop Gly30–Gly33 (Fig. 1) was modelled into two discrete conformations. Furthermore, 37 side chains and 28 peptide bonds are modelled in alternate conformations. Surprisingly, there is no second calcium ion in the trigonal form of the atomic resolution model, which may be a consequence of the alternate conformation adopted by the side-chain atoms of residue Glu92. During the progress of the refinement, we observed a large positive density (more than 6σ) in the place where a chloride ion was located in earlier structures (Steiner *et al.*, 2001; Sekar *et al.*, 2005, 2006) and interpreted it as a chloride ion. A total of 253 water sites were identified, of which 25 were modelled with alternate positions with the sum of their occupancies fixed to 1.0 during the refinement. 200 water sites are in the first hydration shell and make 178 and 235 hydrogen bonds (<3.6 Å) with the polar atoms of the main chain and side chain, respectively. The average *B* factor is 15 Å^2 for the parts of the molecule corresponding to well defined secondary structure and the highest temperature factors (three times more than those of the ordered region) are found in the flexible regions (surface loop, calcium-binding loop and C-terminal region). A comparison of the monoclinic and trigonal form of the quadruple-mutant structures with other related structures is carried out. The backbone atoms of all the structures are superposed and the most visibly deviating regions are located in three segments: the surface loop (residues 60–70), the primary calcium-binding loop (residues 30–34) and the C-terminal region (residues 113–123).

3.3. Surface loop

In most of the bovine pancreatic PLA_2 and mutant structures reported to date (Huang *et al.*, 1996; Sekar *et al.*, 1997, 1999; Yu *et al.*, 2000), the surface-loop residues are always found to be disordered, except for the orthorhombic forms of the wild type (Sekar & Sundaralingam, 1999; Steiner *et al.*, 2001) and the monoclinic forms of the triple mutants K56,120,121M (Rajakannan *et al.*, 2002) and K53,56,121M (Sekar *et al.*, 2005). In the present monoclinic form, the surface loop is also ordered and the electron density is very clear. Furthermore, part of the surface loop (residues 62–66) adopts unique conformations similar to those in the triple mutants K56,120,121M (Rajakannan *et al.*, 2002) and K53,56,121M (Sekar *et al.*, 2005). In contrast, the surface loop is disordered in the trigonal quadruple-mutant structure. Despite the improvement of resolution and the fact that the data were collected at low temperature, the surface loop remains flexible. This is mainly a consequence of the absence of the second calcium ion in the trigonal form of the quadruple-mutant structure.

In order to understand the unique conformation of the surface loop observed in all structures where the second calcium ion is present, superposition of the four structures [the current monoclinic form, the two triple mutants (Rajakannan *et al.*, 2002; Sekar *et al.*, 2005) and the orthorhombic form of the wild type (Sekar & Sundaralingam, 1999)] with ordered surface-loop residues was carried out and is shown in Fig. 4. Note that the second calcium ion is present in the first three structures but is absent in the wild-type orthorhombic form and the latter shows a different conformation in its surface loop even though it is ordered. Interestingly, the side-chain conformation of the residues Lys62 and Asp66 are completely different in the structures containing the second calcium ion (cyan colour in Fig. 4) compared with that observed in the absence of the second calcium ion (red colour in Fig. 4). In support of the above point, biochemical studies indicated that the ordering of the surface loop is essential for effective binding of the enzyme to the membrane (Kuipers *et al.*, 1989).

3.4. Role of the second calcium

The second calcium ion is observed in the monoclinic form of the quadruple-mutant structure. In addition, the surface loop is ordered and part of it (residues 62–66) adopts a unique conformation similar to other structures containing the second calcium ion. As suggested in our previous work, the conformational variation of the surface loop is induced by the second calcium ion (Rajakannan *et al.*, 2002) and the altered loop in turn brings the charged residues Lys62 and Asp66 into the direct vicinity of the second calcium cleft. Previous biochemical studies with porcine PLA_2 indicated that the catalytic rates are significantly higher in the second calcium-bound structures (van den Bergh *et al.*, 1989) and that the second calcium ion is responsible for effective interaction with organized lipid–water interfaces (van Dam-Mieras *et al.*, 1975). Furthermore, van den Bergh and coworkers stated that the charge neutralization by binding of extra calcium ion obviously improves the affinity of the enzyme for aggregated substrates (van den Bergh *et al.*, 1989). As has been pointed out, the ordering of the surface loop is essential for effective binding of the enzyme to the membrane (Verger, 1976; Verger *et al.*, 1973). Based on the mounting evidence from structural and functional studies, we believe that the second calcium ion and some of the residues from the surface loop are necessary for effective interaction of the enzyme with the membrane assembly and decided to undertake a docking study for membrane–enzyme interaction involving the second calcium. Previously, site-selective spin-labelling and electron-para-

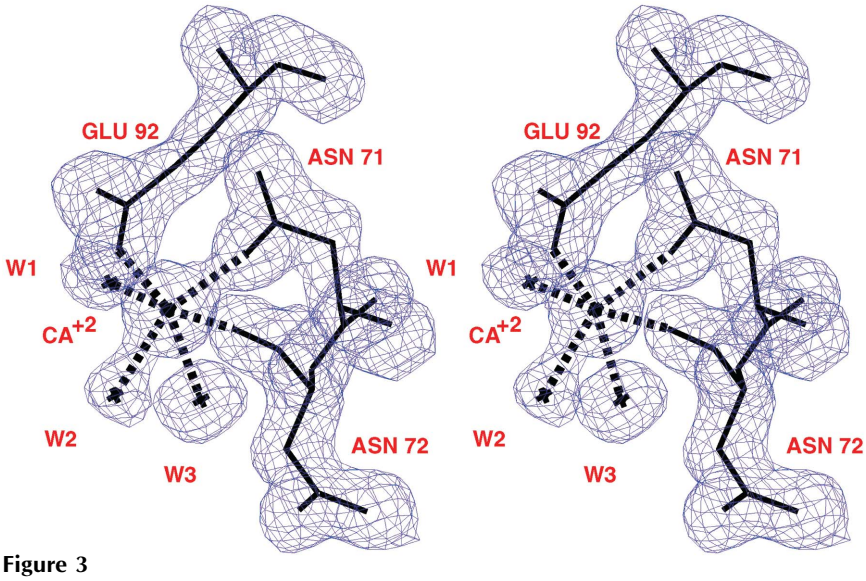

Figure 3
A stereoview of the omit electron-density map showing the second calcium ion (molecule *A* only) and its liganded atoms. Contours are shown at the 1.0σ level.

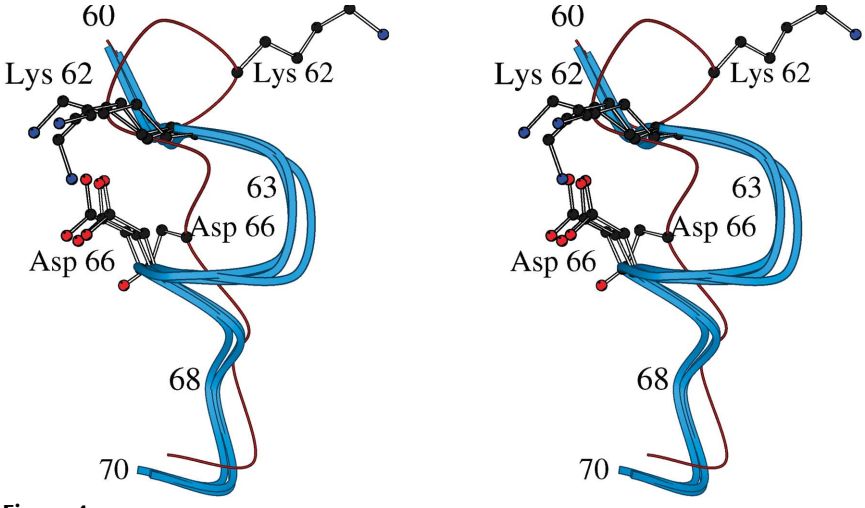

Figure 4
A stereoview of the superposition (Sumathi *et al.*, 2006) of the surface loops (residues 60–70) from four crystal structures showing the conformational variation. The three conformations (cyan) are from structures in which the second calcium is present (the current monoclinic form and two triple mutants; Rajakannan *et al.*, 2002; Sekar *et al.*, 2005). In contrast, the loop shown in red was observed in the orthorhombic form of the wild type where there is no second calcium ion. The side chains of residues Lys62 and Asp66 are also shown.

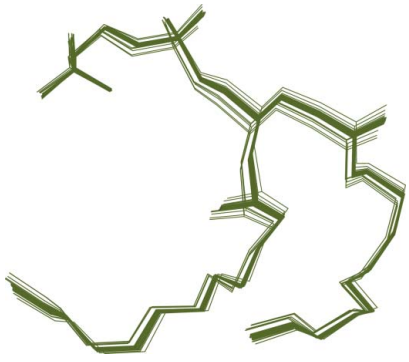

Figure 5
Ensemble of conformations (99) having minimum docking energy in the most populated cluster (40%).

magnetic studies indicated that during interfacial binding the enzyme PLA_2 sits on the membrane (Lin *et al.*, 1998), but the residues involved and the nature of interactions with the membrane phospholipid are yet to be established.

With these basic facts, docking of a phospholipid molecule to the second calcium ion has been carried out. The atomic coordinates of the phospholipid molecule were obtained from the PDB (PDB code 1lpa). The PLA_2–lipid model was subjected to automated docking simulation using the program *AutoDock* 3.0.5 (Morris *et al.*, 1998). The *INSIGHT II* package was used to generate the necessary input files for docking. Atomic energy grids were calculated at 0.375 Å positioned in a 60 Å cubic box centred on the lipid molecule. Simulation was allowed to run for 250 runs (each run consists of 50 cycles) using a genetic algorithm. All the crystallographic water molecules were removed during docking. The program gave one best conformation for each run. Out of the 250 best (with minimum energy) conformations, 40% of them (99 out of 250) were clustered (Fig. 5) in a group with lowest negative docked energy. Interestingly, all the conformations in this cluster showed substantial conservation of interactions with the protein molecule including the second calcium ion. One of the best conformations (highest ranked) of the lipid molecule has been selected from the cluster as a representative and is shown in Fig. 6. It is clear that the polar atoms of the head group of the lipid molecule are interacting with the second calcium ion and the surface-loop residues (Fig. 7). Furthermore, a transition-state analogue has been included in the above suggested model to show that both the transition-state analogue (blue colour) and the phospholipids (green colour) are on the same side and fit well into the interface (Fig. 8). The atomic coordinates of the transition-state analogue were extracted from earlier work (Sekar, Kumar *et al.*, 1998) and were placed in the active site by maintaining the interactions found in the original structure (PDB code 1mkv). The modelling study suggests that the interactions of the polar head group of the membrane phospholipids with the enzyme at the i-face could involve the second calcium ion and the charged residues from the surface loop (Lys62 and Asp66). We hypothesize that the two structures of the quadruple mutant in the monoclinic and trigonal systems could represent the conformations of PLA_2 at the lipid interface and in solution, respectively.

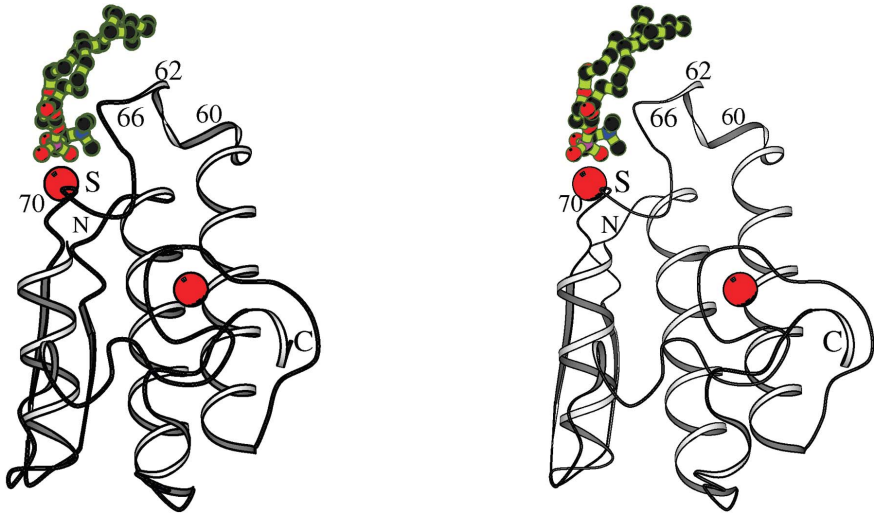

Figure 6
A stereoview of the ribbon model of the present monoclinic quadruple mutant and the second calcium ion (S). The docked phospholipid molecule (green colour) is also shown in ball-and-stick representation.

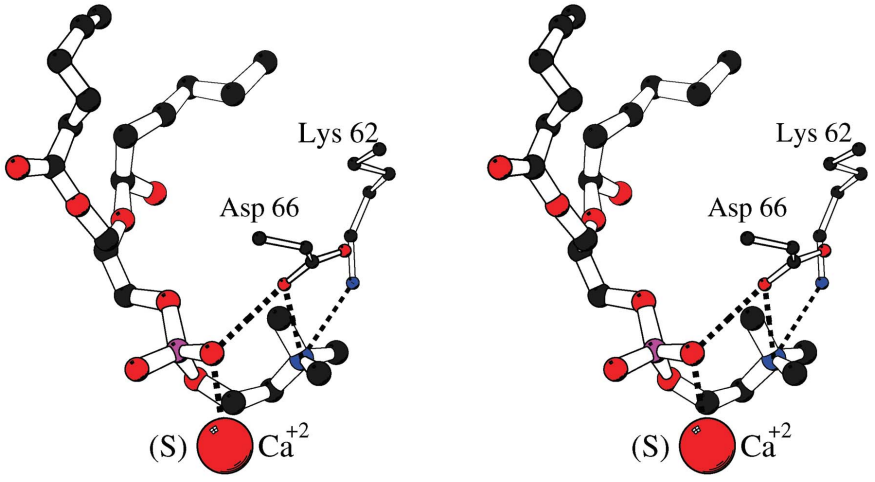

Figure 7
Stereoview showing detailed interactions between the docked lipid molecule and the second calcium. One of the phosphate anionic O atoms of the modelled phospholipid molecule is involved in the second calcium ion coordination. In addition, it is also hydrogen bonded to the carboxylate O atom of Asp66. Furthermore, the N atom of the phosphatidylcholine is hydrogen bonded to Lys62 and Asp66. For clarity, only the residues which are involved in the interactions are shown. Furthermore, the last six C atoms of the long acyl chains are omitted in the drawing for clarity.

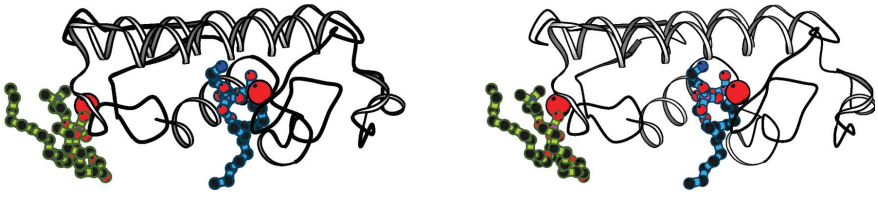

Figure 8
A transition-state analogue molecule (blue colour) is modelled in Fig. 6 with the primary calcium ion.

4. Conclusions

The crystal structures of the quadruple mutant with and without the second calcium reveal flexible surface-loop dynamics and suggest the possibility that the second calcium ion interacts with phospholipid head groups in the interfacial binding. A docked structure suggests that the head group of the phospholipid at the interface could interact with the second calcium ion and with the surface-loop residues Lys62 and Asp66. These studies suggest that the second calcium and the conformational variation in the surface loop are important factors in positioning the PLA_2 enzyme at the membrane–water interface. This is a novel feature for the interfacial binding of PLA_2, but it remains to be further tested experimentally.

The medium-resolution intensity data were collected at the National X-ray data-collection facility at the Molecular Biophysics Unit, Indian Institute of Science, Bangalore, India, supported by the Department of Science and Technology (DST) and the Department of Biotechnology (DBT), India. The facilities at the Supercomputer Education and Research Centre, the Bioinformatics Centre and the Interactive Graphics Molecular Modelling Facility are gratefully acknowledged. DV thanks UGC and DST for funding. The authors thank Mirka Dauter for her help in data collection. The work from Dr Tsai's laboratory is supported by NIH grant GM 57568 and by the Genomics Research Center. AS is supported by a CSIR fellowship. The authors thank an anonymous referee for useful suggestions. This work was supported in part by the Intramural Research program of the National Cancer Institute, Center for Cancer Research.

References

Berg, O. G., Gelb, M. H., Tsai, M.-D. & Jain, M. K. (2001). *Chem. Rev.* **101**, 2613–2654.
Bergh, C. J. van den, Bekkers, A. C., Verheij, H. M. & de Haas, G. H. (1989). *Eur. J. Biochem.* **182**, 307–313.
Brünger, A. T. (1992). *Nature (London)*, **355**, 472–474.
Brünger, A. T., Adams, P. D., Clore, G. M., DeLano, W. L., Gros, P., Grosse-Kunstleve, R. W., Jiang, J.-S., Kuszewski, J., Nilges, M., Pannu, N. S., Read, R. J., Rice, L. M.,

Simonson, T. & Warren, G. L. (1998). *Acta Cryst.* D**54**, 905–921.
Dam-Mieras, M. C. van, Slotboom, A. J., Pieterson, W. A. & de Haas, G. H. (1975). *Biochemistry*, **14**, 5387–5394.
Deng, T., Noel, J. P. & Tsai, M.-D. (1990). *Gene*, **93**, 229–234.
Dennis, E. A. (1994). *J. Biol. Chem.* **269**, 13057–13060.
Dijkstra, B. W., Kalk, K. H., Drenth, J., de Haas, G. H., Egmond, M. R. & Slotboom, A. J. (1984). *Biochemistry*, **23**, 2759–2766.
Engh, R. & Huber, R. (1991). *Acta Cryst.* A**47**, 392–400.
Huang, B., Yu, B.-Z., Rogers, J., Byeon, I. J., Sekar, K., Chen, X., Sundaralingam, M., Tsai, M.-D. & Jain, M. K. (1996). *Biochemistry*, **35**, 12164–12174.
Jain, M. K., Rogers, J., Jahagirdar, D. V., Marecek, J. F. & Ramirez, F. (1986). *Biochim. Biophys. Acta*, **860**, 435–447.
Jones, T. A. (1985). *Methods Enzymol.* **115,** 157–171.
Kissinger, C. R., Gehlhaar, D. K. & Fogel, D. B. (1999). *Acta Cryst.* D**55**, 484–491.
Kraulis, P. J. (1991). *J. Appl. Cryst.* **24**, 946–950.
Kuipers, O. P., Dijkman, R., Pals, C. E., Verheij, H. M. & de Haas, G. H. (1989). *Protein Eng.* **2**, 467–471.
Laskowski, R. A., MacArthur, M. W., Moss, D. S. & Thornton, J. M. (1993). *J. Appl. Cryst.* **26**, 283–291.
Lin, Y., Nielsen, R., Murray, D., Hubbell, W. L., Mailer, C., Robinson, B. H. & Gelb, M. H. (1998). *Science*, **279**, 1925–1929.
Minor, W. (1993). *XDISPLAYF Program.* Purdue University, West Lafayette, IN, USA.
Morris, G. M., Goodsell, D. S., Halliday, R. S., Huey, R., Hart, W. E., Belew, R. K. & Olson, A. J. (1998). *J. Comput. Chem.* **19**, 1639–1662.
Navaza, J. (1994). *Acta Cryst.* A**50**, 157–163.
Otwinowski, Z. (1993). *Proceedings of the CCP4 Study Weekend. Data Collection and Processing*, edited by L. Sawyer, N. Isaacs & S. Bailey, pp. 56–62. Warrington: Daresbury Laboratory.
Otwinowski, Z. & Minor, W. (1997). *Methods Enzymol.* **276**, 307–326.
Peters, A. R., Dekker, N., van den Berg, L., Boelens, R., Kaptein, R., Slotboom, A. J. & de Haas, G. H. (1992). *Biochemistry*, **31**, 10024–10030.
Rajakannan, V., Yogavel, M., Poi, M.-J., Jeyaprakash, A. A., Jeyakanthan, J., Velmurugan, D., Tsai, M.-D. & Sekar, K. (2002). *J. Mol. Biol.* **324**, 755–762.
Ramachandran, G. N. & Sasisekharan, V. (1968). *Adv. Protein Chem.* **23**, 283–438.
Rogers, J., Yu, B.-Z., Tsai, M.-D., Berg, O. G. & Jain, M. K. (1998). *Biochemistry*, **37**, 9549–9556.
Scott, D. L., White, S. P., Otwinowski, Z., Yuan, W., Gelb, M. H. & Sigler, P. B. (1990). *Science*, **250**, 1541–1546.
Sekar, K., Biswas, R., Li, Y., Tsai, M.-D. & Sundaralingam, M. (1999). *Acta Cryst.* D**55**, 443–447.
Sekar, K., Gayathri, D., Velmurugan, D., Jeyakanthan, J., Yamane, T., Poi, M.-J. & Tsai, M.-D. (2006). *Acta Cryst.* D**62**, 392–397.
Sekar, K., Kumar, A., Liu, X., Tsai, M.-D., Gelb, M. H. & Sundaralingam, M. (1998). *Acta Cryst.* D**54**, 334–341.
Sekar, K., Rajakannan, V., Gayathri, D., Velmurugan, D., Poi, M.-J., Dauter, M., Dauter, Z. & Tsai, M.-D. (2005). *Acta Cryst.* F**61**, 3–7.
Sekar, K., Sekharudu, C., Tsai, M.-D. & Sundaralingam, M. (1998). *Acta Cryst.* D**54**, 342–346.
Sekar, K. & Sundaralingam, M. (1999). *Acta Cryst.* D**55**, 46–50.
Sekar, K., Vaijayanthi Mala, S., Yogavel, M., Velmurugan, D., Poi, M.-J., Vishwanath, B. S., Gowda, T. V., Jeyaprakash, A. A. & Tsai, M.-D. (2003). *J. Mol. Biol.* **333**, 367–376.
Sekar, K., Yu, B.-Z., Rogers, J., Lutton, J., Liu, X., Chen, X., Tsai, M.-D., Jain, M. K. & Sundaralingam, M. (1997). *Biochemistry*, **36**, 3104–3114.
Shanthi, V., Rajesh, C. K., Jayalakshmi, J., Vijay, V. G. & Sekar, K. (2003). *J. Appl. Cryst.* **36**, 167–168.
Sheldrick, M. & Schneider, T. R. (1997). *Methods Enzymol.* **277**, 319–343.
Steiner, R. A., Rozeboom, H. J., de Vries, A., Kalk, K. H., Murshudov, G. N., Wilson, K. S. & Dijkastra, B. W. (2001). *Acta Cryst.* D**57**, 516–526.
Sumathi, K., Ananthalakshmi, P., Roshan, M. N. A. M. & Sekar, K. (2006). In the press.
Thanki, N., Thornton, J. M. & Goodfellow, J. M. (1988). *J. Mol. Biol.* **202**, 637–657.
Thunnissen, M. M., Franken, P. A., de Haas, G. H., Drenth, J., Kalk, K. H., Verheij, H. M. & Dijkstra, B. W. (1993). *J. Mol. Biol.* **232**, 839–855.
Verger, R. (1976). *Annu. Rev. Biophys. Bioeng.* **5**, 77–117.
Verger, R., Mieras, M. C. & de Haas, G. H. (1973). *J. Biol. Chem.* **248**, 4023–4034.
Yu, B.-Z., Poi, M.-J., Ramagopal, U. A., Jain, R., Ramakumar, S., Berg, O. G., Tsai, M.-D., Sekar, K. & Jain, M. K. (2000). *Biochemistry*, **39**, 12312–12323.